

CARNet: A Dynamic Autoencoder for Learning Latent Dynamics in Autonomous Driving Tasks

Andrey Pak¹, *Student Member, IEEE*, Hemanth Manjunatha¹, *Student Member, IEEE*
Dimitar Filev², *Fellow, IEEE*, Panagiotis Tsiotras¹, *Fellow, IEEE*

Abstract—Autonomous driving has received a lot of attention in the automotive industry and is often seen as the future of transportation. Passenger vehicles equipped with a wide array of sensors (e.g., cameras, front-facing radars, LiDARs, and IMUs) capable of continuous perception of the environment are becoming increasingly prevalent. These sensors provide a stream of high-dimensional, temporally correlated data that is essential for reliable autonomous driving. An autonomous driving system should effectively use the information collected from the various sensors in order to form an abstract description of the world and maintain situational awareness. Deep learning models, such as autoencoders, can be used for that purpose, as they can learn compact latent representations from a stream of incoming data. However, most autoencoder models process the data independently, without assuming any temporal interdependencies. Thus, there is a need for deep learning models that explicitly consider the temporal dependence of the data in their architecture. This work proposes CARNet, a Combined dynAMic autoencoder NETwork architecture that utilizes an autoencoder combined with a recurrent neural network to learn the current latent representation and, in addition, also predict future latent representations in the context of autonomous driving. We demonstrate the efficacy of the proposed model in both imitation and reinforcement learning settings using both simulated and real datasets. Our results show that the proposed model outperforms the baseline state-of-the-art model, while having significantly fewer trainable parameters.

Index Terms—Autonomous vehicles, Autoencoders, Imitation Learning, Reinforcement Learning.

I. INTRODUCTION

Reinforcement Learning (RL) and Imitation Learning (IL) have been gaining much traction in the area of autonomous driving as a promising avenue to learn an end-to-end policy, which directly maps sensor observations to steering and throttle commands. However, approaches based on RL or IL require many training samples collected from a multitude of sensors of different modalities, including camera images, LiDAR scans, and Inertial-Measurement-Units (IMUs). These data modalities generate high-dimensional data that are both spatially and temporally correlated. In order to effectively use the information collected from the various sensors and develop an abstract description of the world, this high-dimensional data needs to be reduced to low-dimensional representations [1]. To this end, Variational Autoencoders (VAEs) have been extensively used in the past to infer low-dimensional *latent variables*.

The VAEs are trained to operate on high-dimensional data through a probabilistic inference process. However, in most autoencoder or VAE models, the data samples are processed independently from each other, without imposing any temporal dependencies, thus resulting in a loss of performance if the data are generated by a dynamic system. Furthermore, modeling temporal dependencies in the data allows to construct a good *prediction model*, which has been shown to benefit RL/IL scenarios [2], [3]. Empirical evidence also suggests that the human brain constructs an internal model of the world that is used to reason about possible futures (what/if/should happen) and then combines the outcome of this prediction with sensory input to form a belief model [4]. For application areas such as autonomous driving, the temporal characteristics of the data are more imperative, as most of the system components involved are dynamic. The problem is much more complex compared to processing static data one step at a time, as other agents (e.g., other vehicles and pedestrians) are also involved and interact with the learning agent. Thus, there is a need for predictive latent representation models that explicitly consider the temporal dependencies of the data.

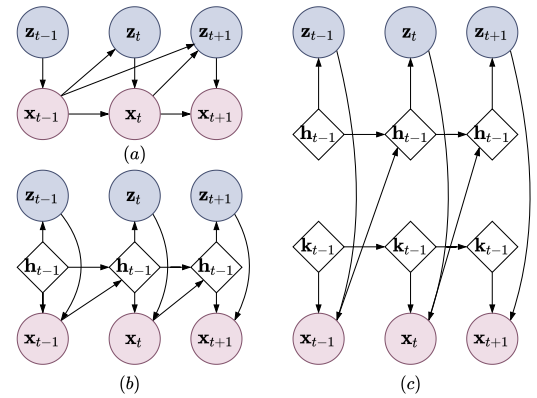


Fig. 1. Two different implementations having same factorization (adapted from [5]). a) The probabilistic graphical model shows the dependency between observed vectors $\mathbf{x}_{1:T}$ and latent vectors $\mathbf{z}_{1:T}$ in terms of a recurrent neural network (RNN) implementation: b) Both \mathbf{x}_t and \mathbf{z}_t share a common hidden state \mathbf{h}_t , however, in c) the \mathbf{x}_t and \mathbf{z}_t are generated using two different hidden vectors, \mathbf{k}_t and \mathbf{h}_t .

Dynamic Autoencoders (DAEs) are suitable to model data that are inherently temporal [5]. Given a sequence of random vectors $\mathbf{x}_{1:T} = \{\mathbf{x}_t \in \mathbb{R}^n\}_{t=1}^T$ and a sequence of latent random vectors $\mathbf{z}_{1:T} = \{\mathbf{z}_t \in \mathbb{R}^n\}_{t=1}^T$ that are assumed to be temporally correlated, DAEs generate the joint distribution *pdf* $p_\theta(\mathbf{x}_{1:T}, \mathbf{z}_{1:T})$, where the θ parameters are usually estimated

through deep learning models [5]. A particular DAE model can impose different conditional assumptions between the observed vectors $\mathbf{x}_{1:T}$ and the latent vectors $\mathbf{z}_{1:T}$. For example, if we assume a first-order Markovian dependency, then \mathbf{x}_t and \mathbf{z}_t depend only on \mathbf{x}_{t-1} and \mathbf{z}_{t-1} , respectively. For more general models, one can accumulate the histories ($\mathbf{x}_{1:t-1}$ and $\mathbf{z}_{1:t-1}$) and use a Recurrent Neural Network (RNN) structure to learn the underlying cross-temporal dependencies [5], [6].

The imposed conditional assumptions do not always directly reflect the implementation details. For instance, consider the following conditional independence structure expressed using the two equations below

$$p(\mathbf{z}_t \mid \mathbf{x}_{1:t-1}, \mathbf{z}_{1:t-1}) = p(\mathbf{z}_t \mid \mathbf{x}_{1:t-1}), \quad (1a)$$

$$p(\mathbf{x}_t \mid \mathbf{x}_{1:t-1}, \mathbf{z}_{1:t}) = p(\mathbf{x}_t \mid \mathbf{x}_{1:t-1}, \mathbf{z}_t). \quad (1b)$$

Here it is assumed that \mathbf{x}_t and \mathbf{z}_t depend on the history $\mathbf{x}_{1:t-1}$ (this independence assumption is shown in Fig. 1a). Naturally, we can use an Recurrent Neural Network (RNN) structure to capture this assumption, while completely differing in terms of the internal network implementation. For example, in Fig. 1b) a single hidden state \mathbf{h}_t is shared between \mathbf{x}_t and \mathbf{z}_t . On the other hand, in Fig. 1c), two different hidden states, namely, \mathbf{k}_t and \mathbf{h}_t are used to model \mathbf{x}_t and \mathbf{z}_t , respectively. Thus, the family of temporal models not only depends on the independence assumptions, but also on the implementation details [5].

Motivated by this observation, we present a combined model for learning the latent space from high-dimensional, temporally correlated data. The proposed combined architecture is shown in Fig. 2. The architecture combines an Autoencoder (AE) and an RNN (in the form of Gated Recurrent Unit (GRU)) in a single network with parameter sharing. Many previous works support the rationale for weight sharing [5], [7]–[9], where it has been shown that weight sharing between a generative model ($p(\mathbf{x}, \mathbf{z})$) and an inference model ($q(\mathbf{z}|\mathbf{x})$) can improve training. Throughout this paper, we refer to this combined model as **Combined dynAmic autoencoder Network (CARNet)**. The CARNet learns to estimate the present latent vector and also predict the future latent vector from raw data. These latent vectors are then used to learn autonomous driving tasks using reinforcement learning.

In addition to the proposed combined architecture to learn latent space representations, we also explore the effect of attention mechanisms [10] on latent vector estimation from images. The reasoning behind this idea is that not all parts of the input image are equally informative, and are not all equally relevant for planning. For instance, recent works [11], [12] have shown that an agent does not have to learn representations that are capable of reconstructing the complete observation; instead, it is sufficient that the representation allows predicting only the quantities that are directly relevant for planning. Ideally, a latent space representation should incorporate only the essential information for the current decision-making task while filtering out all the unnecessary details. For example, while driving, a driver’s attention shifts toward an adjacent lane while performing a lane change. By focusing on the adjacent lane, the driver discards irrelevant objects and obser-

vations, thus reducing the unnecessary complexity of scene understanding, which facilitates efficient decision-making [13], [14]. We explore the use of attention to filter out unnecessary parts of the image for latent vector estimation.

Contributions

We present a new **Combined dynAmic autoencoder Network (CARNet)** that learns current and future latent representations from raw high-dimensional data and, in addition, acts as a future latent vector prediction model. In contrast to similar state-of-the-art end-to-end driving architectures (e.g., [6]), our approach has the benefits of sharing the parameters between the AE and the RNN, which is shown to increase performance. Due to the architecture of the proposed model, latent vector learning has additional continuity constraints, which enables a smooth transition between latent vectors. In addition, the proposed model has significantly fewer (≈ 2.5 times) number of parameters than the selected baseline state-of-the-art model. We validate the efficacy of the proposed model in two sets of experiments using imitation learning and reinforcement learning. The results show that the proposed model outperforms the baseline (e.g., [6]), while having significantly fewer parameters.

II. RELATED WORK

Knowing how the environment may evolve in the immediate future is crucial for the successful and efficient planning of an agent interacting with a complex environment. Traditionally, this problem has been approached using Model-Predictive Control (MPC) along with system identification [15]. While these classical approaches are powerful and well-established tools when the dynamical model is known and relatively simple, in practice it becomes increasingly difficult to apply these techniques to more realistic and complex problems, such as autonomous driving. Recently, driven by computer hardware advancements, along with the use of computational algorithms that harvest the expressivity and generalizability of deep neural network architectures, it has become possible to learn representations of complex and realistic environments. This section gives an overview of the current approaches addressing learning, simulating, and predicting dynamic environments.

Recurrent Neural Networks (RNNs) are one of the most popular architectures frequently used to model time-series data. The idea of using RNNs for learning the system dynamics and making future predictions, as well as for simulating previously observed environments, has recently gained popularity [16]–[19]. The capability of encoding/generative models, combined with the predictive capabilities of the recurrent networks, provides a promising framework for learning complex environment dynamics. In this regard, Girin et al., [5] provide a broad overview of available methods that model the temporal dependencies within a sequence of data and the corresponding latent vectors. This overview covers the recent advancements in learning and predicting environments such as basic video games and frontal-camera autonomous driving scenarios based on the combination of an autoencoder and a recurrent network.

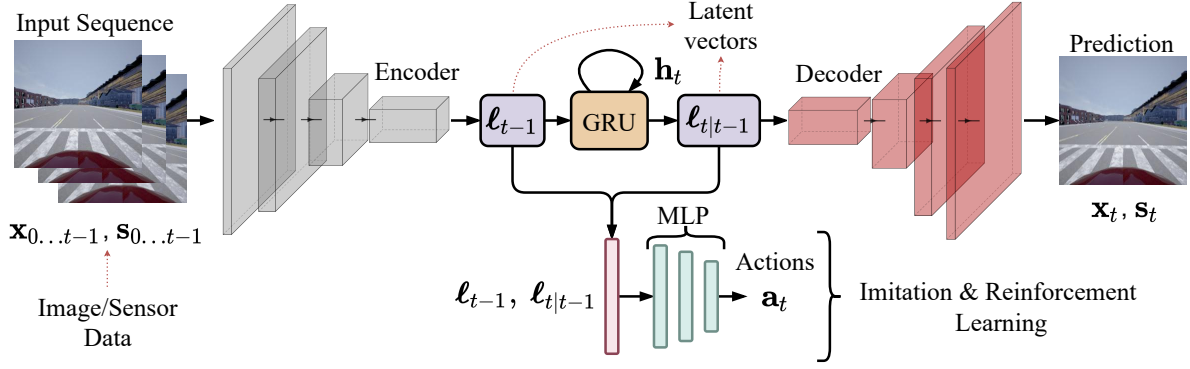


Fig. 2. Overview of the CARNet architecture with imitation and reinforcement learning. The proposed CARNet combines both the encoder and decoder networks with a recurrent neural network to learn present and future latent vectors. These latent vectors are used to learn autonomous driving tasks using reinforcement learning.

Generative recurrent neural network architectures have also been used in simulators. In [20] the authors propose a recurrent neural network-based simulator that learns action-conditional based dynamics that can be used as a surrogate environment model while decreasing the computational burden. The RNN simulator was shown to handle different environments and capture long-term interactions. The authors also show that state-of-the-art results can be achieved in Atari games and a 3D Maze environment using a latent dynamics model that is learned from observing both human and AI playing. The authors also highlighted the limitations of the proposed RNN architecture for learning more complex environments (such as 3D car racing and 3D Maze navigation) and identified the existing trade-offs between long and short-term prediction accuracy. They also discussed and compared the implications of prediction/action/observation dependent and independent transitions.

One of the most influential works along the lines of environment modeling for RL tasks is the World Models (WM) by Ha and Schmidhuber [6]. They propose to model the world dynamics using VAE and RNN in a reinforcement learning context. They showed how spatial and temporal features extracted from the environment in an unsupervised manner could be successfully used to infer the desired control input, and how they can yield a policy that is sufficient for solving typical RL benchmarking tasks in a simulated environment. The proposed WM architecture consists of three parts. First, a VAE is used to learn the latent representation of several simulated environments (e.g., Car Racing and VizDoom). Second, a Mixture Density Network (MDN)-RNN [21] performs state predictions based on the learned latent variable and the corresponding action input. Finally, a simple Multi-Layer Perceptron (MLP) determines the control action from the latent variables. The authors achieved state-of-the-art performance from training the model both in an actual environment and the simulated latent space, i.e. the “dream” generated by sampling the VAE’s probabilistic component. In VizDoom [22] the model, which was trained purely in the simulated environment (i.e., the “dream”), was able to apply its experience to the real game environment and even take advantage of the inherent flaws of the game. The central intuition behind the WM approach

is that living beings develop an internal perception model of the outside world based on their sensory inputs, which is then used for everyday activities. The WM architecture inspired the proposed model in the sense that we also use a combination of an AE and an RNN. We improved the baseline WM approach by enabling parameter sharing, that has been shown [5], [7]–[9] to increase the quality of learning the dynamic transitions. Additional losses are introduced to improve latent space continuity, and the overall size and complexity of the combined architecture is reduced.

In [23] the same authors as in [6] addressed the challenge of learning the latent dynamics of an unknown environment. The proposed PlaNet architecture uses image observations to learn a latent dynamics model and then subsequently performs planning and action choice in the latent space. The latent dynamics model uses both deterministic and stochastic components in a recurrent architecture to improve the planning performance.

In a similar study from Nvidia, GameGAN [24] proposed a generative model that learns to visually imitate the desired game by observing screenplay and keyboard actions during training. Given the gameplay image and the corresponding keyboard input actions, the network learned to imitate that particular game. The approach in [24] can be divided into three main parts: the Dynamics Engine, an action-conditioned Long-Short Term Memory (LSTM) [20], [25] that learns action-based transitions; the external Memory Module, whose objective is to capture and enforce long-term consistency; and the Rendering Engine that renders the final image not only by decoding the output hidden state but also by decomposing the static and dynamic components of the scene, such as the background environment vs. moving agents. The authors achieve state-of-the-art results for some game environments such as Pacman and VizDoom [22].

The recent DriveGAN [26] approach proposes a scalable, fully-differentiable simulator that also learns the latent representation of a given environment. The latent representation part of the DriveGAN uses a combination of β -VAE [27] for inferring the latent representation and StyleGAN [28], [29] for generating an image from the latent vector. This approach has an advantage over classic VAE, as in this case a similarity

metric between the produced images is also learned during the training process [30]. Like the WM, StyleGAN uses a pre-training step to learn the latent space. Afterwards, the network is used to learn the connection between the actual latent representations and the corresponding actions taken between the transitions using the custom Dynamic Engine architecture that learns the transitions between latent vectors. The Generative Adversarial Network (GAN) component improves the image decoding qualities and can make sharper reconstructions compared to an exclusively convolutional decoder. The last two GAN-based approaches mostly explore generational capabilities of the proposed architectures in simulating the future state based on previous image and action sequences. However, these architectures can be adapted directly in the context of RL or imitation learning.

In summary, all current state-of-the-art techniques use two main components to perform accurate future predictions: first, an unsupervised pre-training step is utilized to learn the latent space of the given environment. This step usually involves an autoencoder or an autoencoder-GAN combination; second, a recurrent network, usually in the form of LSTM is used to capture the spatio-temporal dependencies in the data and make future predictions based on the previously observed frames and action inputs. However, most of these prior works train the autoencoder and recurrent architectures separately, with one of the main reasons being the training speed. While this training approach is perfectly reasonable and achieves state-of-the-art results, the learned latent representation is static. Moreover, some dynamic relations captured by the recurrent part might not be rich-enough. On the contrary, in this paper, we combine the autoencoder and recurrent architectures into a single architecture that is trained simultaneously and outperforms the baseline network where these parts are trained separately.

III. APPROACH

Our main objective is to use the capability of a combined AE-RNN architecture to make accurate predictions of future states using latent representations. The proposed approach is inspired by the World Models (WM) [6] architecture. However, in contrast with WM, where the VAE and RNN do not share any parameters, in our approach the AE and RNN networks are trained together. Also, instead of a VAE, we use an AE architecture. The first reason behind choosing an AE rather than a VAE architecture stems from our desire to explore the minimum possible configuration of the network; adding a Gaussian mixture model to produce the latent variable would increase the number of parameters. The second reason is to avoid “dream” training that may lead to adversarial policies, where the probabilistic model “cheats” the environment by generating trajectories that do not follow the laws governing the actual environment [6]. In the context of autonomous driving, such trajectories are unacceptable for safety concerns.

A. CARNet Architecture

The overall architecture of the proposed CARNet is shown in Fig. 3. The main intuition behind training together the AE and GRU networks is as follows: while the autoencoder

itself provides sufficient capabilities for capturing the latent state and reconstructing the subsequent images, it may omit temporal dependencies that are necessary for the proper prediction of the latent variable. Additionally, it is possible to further enforce temporal continuity in the latent space by introducing additional losses. In addition to operating purely on latent vectors, the architecture can also incorporate sensor measurements in the latent/hidden vectors (see Fig. 3). The rationale is that images alone are not sufficient to capture complex environments (e.g., driving) and additional inputs may be needed. Moreover, autonomous vehicles are already equipped with a wide array of sensors that can be used to sense the environment.

TABLE I
AUTOENCODER STRUCTURE

Encoder		Decoder	
Layer	Output Shape	Layer	Output Shape
Input	1x256x256	Input	1x128
conv3-2	2x128x128	tconv3-64	64x4x4
conv3-2		tconv3-64	
conv3-4	4x64x64	tconv3-32	32x8x8
conv3-4		toconv3-32	
conv3-8	8x32x32	tconv3-16	16x16x16
conv3-8		tconv3-16	
conv3-16	16x16x16	tconv3-8	8x32x32
conv3-16		tconv3-8	
conv3-32	32x8x8	tconv3-4	4x64x64
conv3-32		tconv3-4	
conv3-64	64x4x4	tconv3-2	2x128x128
conv3-64		tconv3-2	
conv3-128	128x1x1	tconv3-1	1x256x256

The architecture of the baseline autoencoder (see Table I) follows a simple/transposed convolution architecture with a kernel size of 3×3 . All convolution layers are followed with a batch normalization layer and a ReLU activation. With the dimension of the input image being 256×256 , the resulting size of the latent variable is 128. During performance comparison, both CARNet and World Models (WM) share identical layer structure, apart from the probabilistic part in VAE.

To better understand the flow of the processing induced by the proposed architecture (Fig. 3), let us consider a sequence of $t + 1$ consecutive frames $[\mathbf{x}_0, \dots, \mathbf{x}_t]$ taken from the frontal camera of a moving vehicle, along with the corresponding sensor data. Note that the subscript 0 refers to the beginning of the current sliding window, and not to the beginning of the dataset. Given the first t frames $[\mathbf{x}_0, \dots, \mathbf{x}_{t-1}]$ and corresponding sensor data $[\mathbf{s}_0, \dots, \mathbf{s}_{t-1}]$, our aim is to learn the latent representations $[\ell_0, \dots, \ell_{t-1}]$ and predict \mathbf{x}_t , ℓ_t , and \mathbf{s}_t . Referring to Fig. 3, and for the sake of simplicity, let us consider a single-step prediction at time step $t - 1$, without any sensor data. The image \mathbf{x}_{t-1} is encoded into the latent variable as $\ell_{t-1} = \mathbf{E}(\mathbf{x}_{t-1})$, where \mathbf{E} denotes the encoder. It is important to mention that in the case where we only propagate the images (i.e., without sensor data), $\dim(\mathbf{h}_t) = \dim(\ell_t)$. Also, note that the encoder/decoder can be any architecture or

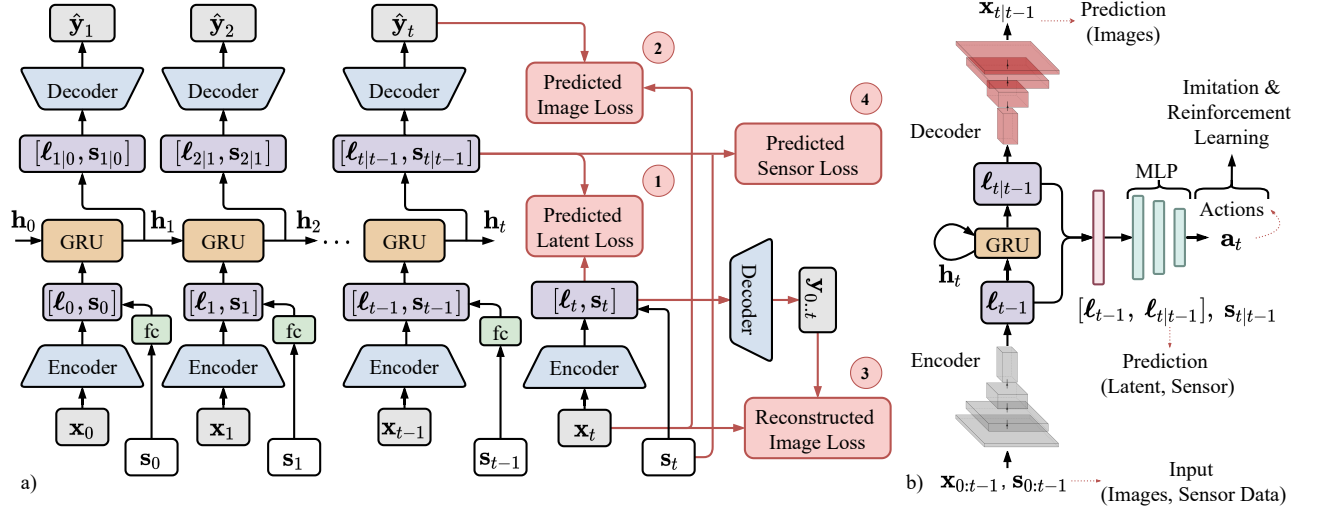


Fig. 3. Combined recurrent architecture. Sequence of images is first encoded into latent space, fused (concatenated) with corresponding sensor measurements, then propagated through the recurrent network and outputs the estimate of both latent state and sensor measurements at timestep t .

a typical convolutional neural network; hence, we assume a general architecture as follows

$$\ell_{t-1} = \mathbf{E}(\mathbf{x}_{t-1}), \quad (2a)$$

$$\mathbf{y}_{t-1} = \mathbf{D}(\ell_{t-1}), \quad (2b)$$

$$\hat{\mathbf{y}}_t = \mathbf{D}(\ell_{t|t-1}). \quad (2c)$$

The encoded vector ℓ_{t-1} is used as the input to the GRU block, whose output is the latent space vector at the next time step $\ell_{t|t-1} = \mathbf{h}_t$, given by

$$z_t = \sigma(W_z [\mathbf{h}_{t-1}, \ell_{t-1}]), \quad (3a)$$

$$r_t = \sigma(W_r [\mathbf{h}_{t-1}, \ell_{t-1}]), \quad (3b)$$

$$\tilde{\mathbf{h}}_t = \tanh(W [\mathbf{h}_{t-1} \odot r_t, \ell_{t-1}]), \quad (3c)$$

$$\mathbf{h}_t = (1 - z_t) \odot \mathbf{h}_{t-1} + z_t \odot \tilde{\mathbf{h}}_t \equiv \ell_{t|t-1}, \quad (3d)$$

where W, W_z, W_r are learnable weights, σ is a sigmoid function, and \odot is the Hadamard product. The predicted latent variable $\ell_{t|t-1}$ is used as the hidden state for the next time step, as well as an input for reconstructing the image at the next time step, $\hat{\mathbf{y}}_t = \mathbf{D}(\ell_{t|t-1})$, where \mathbf{D} denotes the decoder (see Eq. (2)). It is important to note here that \mathbf{h}_{t-1} also contains information about \mathbf{h}_{t-2} . Thus, the predicted latent vector ℓ_t at time step t not only depends on ℓ_{t-1} , but also on ℓ_{t-2} as per Eq. (3a), and in the case of image data only, no action or sensor conditioning is present.

In the case where sensor data is used, this data is fed through a single fully-connected layer and concatenated with the latent image encoding at each time step. The hidden vector is given as $\mathbf{h} \triangleq [\ell, W_s \mathbf{s}]$ where ℓ and \mathbf{s} are latent and sensor data vectors and W_s are weights that scale the sensor data appropriately. To summarize, we train the CARNet network to model the following transitions:

- In case of image-based latent representation only (Fig. 3, omitting the sensor input \mathbf{s} and the loss (4)), the model

is trained to represent the transition $T(\ell_t | \ell_{t-1}, \mathbf{h}_{t-1})$, or, $T(\ell_t | \ell_{t-1}, \ell_{t-1|t-2})$.

- In case of an augmented latent representation (image + sensor, Fig. 3), the model is trained to represent the transition $T(\ell_t | \ell_{t-1}, \mathbf{s}_{t-1}, \mathbf{h}_{t-1})$, or $T(\ell_t | \ell_{t-1}, \mathbf{s}_{t-1}, [\ell_{t-2}, W_s \mathbf{s}_{t-2}])$ as $\mathbf{h} \triangleq [\ell, W_s \mathbf{s}]$ where the sensor data is passed through a fully-connected layer designated as W_s rather than being concatenated directly to the latent space. The main reasoning for not directly concatenating the latent vector (ℓ) with sensor data (\mathbf{s}) is that the sensor data might not be of same scale as the latent vector. Hence, we use a fully connected layer with weights W_s to scale the sensor data appropriately.

It is important to note that the modeled recurrent network transition is different from the one in World Models (WM) [6]. In WM, the Mixture Density Recurrent Neural Network (MDN-RNN) action-conditioned state transition is defined as $T(\mathbf{z}_t | \mathbf{a}_{t-1}, \mathbf{z}_{t-1}, \mathbf{h}_t)$, where \mathbf{z}_{t-1} and \mathbf{z}_t are the previous and predicted latent states, \mathbf{a}_t is the set of previous actions, and \mathbf{h}_{t-1} is the predicted hidden state of the MDN-RNN. On the other hand, we do not condition the latent state prediction on previous actions i.e., CARNet learns $T(\mathbf{z}_t | \mathbf{z}_{t-1}, \mathbf{h}_t)$ or $T(\mathbf{z}_t | \mathbf{s}_{t-1}, \mathbf{z}_{t-1}, \mathbf{h}_t)$, in case sensor data is used alongside with camera images. However, action information can be added if necessary. In that case, the CARNet model represents the transition $T(\mathbf{z}_t | \mathbf{z}_{t-1}, \mathbf{h}_t, \mathbf{s}_{t-1}, \mathbf{a}_{t-1})$.

B. Training

For training, the overall loss function for the single-step prediction can be broken down into three terms given as

follows

$$L_{\text{total}} = \underbrace{\frac{1}{n+1} \sum_{t=0}^n [L_{\text{MS-SSIM}}(\mathbf{x}_t, \mathbf{y}_t)] + \frac{1}{n} \sum_{t=1}^n [L_{\text{MS-SSIM}}(\mathbf{x}_t, \hat{\mathbf{y}}_t)]}_{\text{Image reconstruction}} + \underbrace{\frac{1}{n} \sum_{t=1}^n L_{1_s}(\ell_{t|t-1}, \ell_t)}_{\text{Latent prediction}} + \underbrace{\frac{1}{n} \sum_{t=1}^n L_{1_s}(\mathbf{s}_{t|t-1}, \mathbf{s}_t)}_{\text{Sensor prediction}}, \quad (4)$$

where ℓ_t , $\ell_{t|t-1}$ denote the encoded latent variable at step t and the conditioned latent prediction, \mathbf{x}_t , \mathbf{y}_t , $\hat{\mathbf{y}}_t$ denote the source and reconstructed image, respectively, where $\hat{\mathbf{y}}_t$ corresponds to the reconstructed image after the GRU (Fig. 3, loss (3)) and \mathbf{y}_t corresponds to ground truth (Fig. 3, loss (2)). For sensor data, \mathbf{s}_t , $\mathbf{s}_{t|t-1}$ represent the ground truth and the predicted sensor qualities, respectively.

In terms of objective functions, a smooth L_1 (L_{1_s}) loss is used for the latent variable (Fig. 3, loss (1)) and the sensor data (Fig. 3, loss (4)). Multi-Scale Structural Similarity Index Measure (MS-SSIM) [31] is used for image prediction to preserve reconstructed image structure and also serves as some form of regularization. In our experiments, using Mean Squared Error (MSE) alone resulted in mode collapse and very blurry reconstructions. SSIM is a similarity measure that compares structure, contrast, and luminance between images. MS-SSIM is a generalization of this measure over several scales [31], as follows

$$L_{\text{MS-SSIM}} = [l_M(\mathbf{x}, \mathbf{y})]^{\alpha_M} \prod_{j=1}^M [c_j(\mathbf{x}, \mathbf{y})]^{\beta_j} [s_j(\mathbf{x}, \mathbf{y})]^{\gamma_j}, \quad (5)$$

where \mathbf{x} and \mathbf{y} are the images being compared, $c_j(\mathbf{x}, \mathbf{y})$ and $s_j(\mathbf{x}, \mathbf{y})$ are the contrast and structure comparisons at scale j , and the luminance comparison $l_M(\mathbf{x}, \mathbf{y})$ (shown in Eq. (6)) is computed at a single scale M , and α_M , and β_j , γ_j ($j = 1, \dots, N$) are weight parameters that are used to adjust the relative importance of the aforementioned components, i.e., contrast, luminance, and structure. These parameters are left to the default implementation values as follows

$$l(\mathbf{x}, \mathbf{y}) = \frac{2\mu_x\mu_y + C_1}{\mu_x^2 + \mu_y^2 + C_1}, \quad (6a)$$

$$c(\mathbf{x}, \mathbf{y}) = \frac{2\sigma_x\sigma_y + C_2}{\sigma_x^2 + \sigma_y^2 + C_2}, \quad (6b)$$

$$s(\mathbf{x}, \mathbf{y}) = \frac{\sigma_{xy} + C_3}{\sigma_x\sigma_y + C_3}. \quad (6c)$$

In (6), μ and σ are the mean and the variance of the image and are treated as an estimate of the luminance and contrast of the image. The constants C_1, C_2, C_3 are given by $C_1 = (K_1L)^2$, $C_2 = (K_2L)^2$, $C_3 = C_2/2$, where L is the dynamic range of the pixels and K_1, K_2 , are two scalar constants. Additionally, not only the final predicted variable is used in the loss function, but all intermediate predictions of the recurrent network are also used in order to improve continuity in the latent space.

C. Separate and Ensemble Training

When pre-training the autoencoder separately on individual images, no temporal relations are captured in the latent space.

This can potentially impact the quality of predictions produced by the RNN network. Since both the autoencoder and the RNN parts are trained together, we did not train the combined architecture from scratch but only pre-trained the autoencoder and then fine-tuned it as part of a bigger network. This resulted in significantly less time spent when training the combined architecture.

D. Attention Mechanism

In addition to the AE-RNN architecture, we also implemented an attention mechanism [10] before the encoder (Fig. 4b). The motivation for the incorporation of the attention mechanism is that not all parts of the image carry relevant information for a particular task. Thus, by adding an attention module, we try to explore whether it results in a performance gain in the AE-RNN model. Since the input in the attention module is an image, we have used the self-attention mechanism for vision models [32].

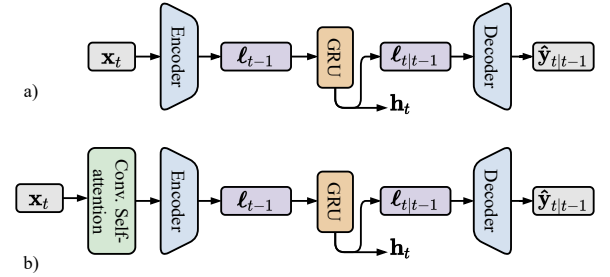


Fig. 4. a) CARNet without attention. b) CARNet with convolution attention mechanism applied to input image.

In terms of self-attention in the image space, given a pixel $x_{ij} \in \mathbb{R}^{d_{in}}$ of the input image x , a local region $ab \in \mathcal{N}_k(i, j)$ around the pixel is extracted with spatial extension k centered at x_{ij} . The output pixel value $y_{ij} \in \mathbb{R}^{d_{out}}$ is calculated using a single-headed self-attention as follows

$$y_{ij} = \sum_{a,b \in \mathcal{N}_k(i,j)} \text{softmax}_{ab} (q_{ij}^\top k_{ab}) v_{ab}, \quad (7)$$

where, $q_{ij} = W_Q x_{ij}$, $k_{ab} = W_K x_{ab}$, and the values $v_{ab} = W_V x_{ab}$ are query, key, and values respectively, with learnable weights W_Q, W_K, W_V . The present formulation can be extended to multi-head attention, with each head having its own learnable parameters by partitioning the pixel features x_{ij} depthwise into N groups. Moreover, the formulation in Eq. (7) does not consider position information to encode attention, which limits the expressiveness in vision tasks. To remedy this, relative attention can be implemented that takes the relative position between the pixel x_{ij} and each element in the region $ab \in \mathcal{N}_k(i, j)$. Thus, the new formulation is given as

$$y_{ij} = \sum_{a,b \in \mathcal{N}_k(i,j)} \text{softmax}_{ab} (q_{ij}^\top k_{ab} + q_{ij}^\top r_{a-i,b-j}) v_{ab}, \quad (8)$$

where $r_{a-i,b-j}$ is the concatenated vector (i.e., $r_{a-i,b-j} = [r_{a-i}, r_{b-i}]$) with row and column position information. Note that the dimension of r_{a-i} and r_{b-i} is $\frac{1}{2}d_{out}$, thus the dimension of $r_{a-i,b-j}$ is d_{out} . More details on self-attention in vision tasks can be found in [32].

E. Simulated Data

In order to learn good latent state representations from image data, a significant amount of data is required. Therefore, the frontal, side, and rear camera images are also included for regularizing and increasing data diversity (e.g., the side camera image becomes similar to the frontal camera image once the vehicle makes a right-angle turn). It is important to note that only the autoencoder part was pre-trained on all camera feeds, and the ensemble network only used the frontal camera. This proved helpful when using real-world datasets with misaligned data, i.e., with the absence of global shutter and mismatching data timestamps. In terms of sensor measurements s_t , we used steering, brake, and throttle data.

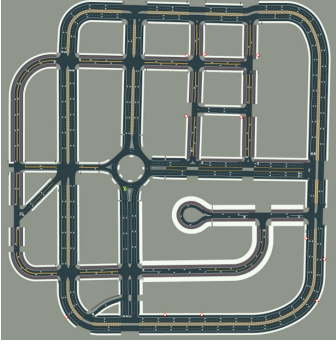


Fig. 5. Map of the town used in CARLA for data generation.

The training data was generated using the CARLA [33] simulator. A total of 300K time steps were generated using random roll-outs (random starting and goal points on the map shown in Fig. 5) utilizing the internal CARLA vehicle autopilot. The simulated data includes 4-directional camera images (front/left/right/rear) along with their corresponding semantic segmentation, IMU and other sensor data (speed, steering, LIDAR, etc.), desired control values, and additional experimental data for auxiliary tasks such as traffic light information.

IV. EXPERIMENTS

We considered two different cases to demonstrate the efficacy of the proposed architecture over the state-of-the-art architectures (e.g., [6]). First, we considered an imitation learning case in which the task is to predict the autopilot actions given the history of states (i.e., a stack of images from the front view camera) for both simulated and real datasets. Imitation learning is cast as a nine-class classification problem where each class corresponds to a unique steering angle and acceleration combination. Note that for imitation learning, neither CARNet nor WM are conditioned on the action history (see Section III-B), as it may lead to bias in the classification. In the second case, we tested the proposed architecture in the CARLA simulator, which provides realistic scenarios in terms of visualization and traffic. For the second RL scenario, CARNet and WM are conditioned on the sensor and action history accordingly (see explanation at the end of Section III-A).

A. Imitation Learning

Annotated data from expert demonstrations have been core drivers in the development and evaluation of learning systems, ranging from computer vision and natural language processing to robotic manipulation tasks and audio processing [34], [35]. The influence of such annotated data is significant in the field of *Imitation Learning*, particularly in game-based platforms. The expert (usually human) demonstrations in such platforms have helped avoid the huge cost of learning from scratch [36], [37] and sometimes even achieve human-level performance. Along the same line of work, we used expert demonstrations to train a neural network in a supervised manner and used the trained neural network as a starting point (“warm starting”) in a reinforcement learning experiment described in Section IV-C below.

For imitation learning, given N autopilot driving sequences $AP_i, i \in (1, \dots, N)$ with corresponding observation frames $I_{i,t}$, we learn a deterministic policy using a network parameterized by θ to mimic the autopilot actions. The action space $A_{i,t}$ contains two continuous actions: steering angle and acceleration. However, for imitation learning, we discretized the continuous values into three levels. The steering angle assumes the values $[-0.2, 0.0, 0.2]$ rad and the acceleration command assumes the values $[-3, 0.0, 3]$ m/s. Imitation learning is set up as a classification problem with nine classes resulting from different combinations of the previous discrete steering and acceleration values. Discretization of the action space is justifiable from a practical perspective, since in autonomous driving applications the high level decision policy derived by imitation learning, reinforcement learning, game theory or some other decision-making techniques is combined with low level trajectory planning and motion control algorithms [38]. For training, we used mean cross-entropy loss between the predicted class and the autopilot class, as follows

$$-\sum_{n=1}^N \sum_{k=1}^K w_k \log \frac{e^{(\mathbf{x}_{n,k})}}{\sum_{i=1}^K e^{(\mathbf{x}_{n,i})}} \mathbf{y}_{n,k}, \quad (9)$$

where N is the total number of autopilot driving sequences, and K is the number of classes.

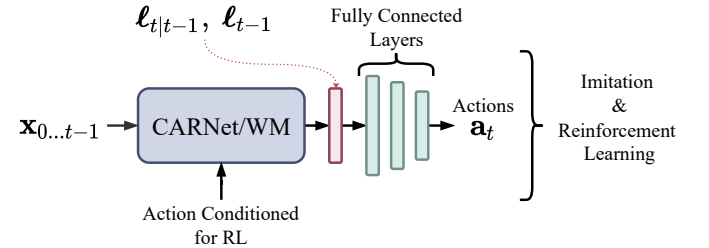


Fig. 6. For imitation learning, CARNet and WM are not conditioned on history of actions. However, for reinforcement learning, both the models are conditioned on the history of actions.

The controller architecture for the imitation learning task consists of a simple four-layer MLP that gradually reduces the dimensionality of the latent space onto the action space (see Fig. 6). The structure of the controller is given in Table II. The controller network uses the stacked previous and predicted

latent vectors, so the input tensor size is twice the chosen latent size $\mathbf{a} = \mathbf{C}([\ell_{t-1}, \ell_t])$, e.g., for a latent size of 128, the size of the input tensor to the imitation learning network is 256.

TABLE II
CONTROLLER STRUCTURE (CARNET)

Layer	Input Size	Output Size
FC1 + ReLU	256	128
FC2 + ReLU	128	128
FC3 + ReLU	128	64
FC4 + ReLU	64	9

The training was performed on a computer equipped with a GeForce RTX3090 GPU, Ryzen 5950x CPU, and 16GB of RAM. Also, the 300K time-steps are split into 70% training, 15% validation, and 15% testing data. The code implementation¹ uses Pytorch with Adam optimizer.

B. Baseline Comparison

Since we drew our inspiration from dynamic autoencoders in general, and World Models in particular, WM is chosen as a baseline comparison network. In WM, the architecture consists of three different parts: a VAE, an MDN-RNN, and a fully connected controller network, which are all trained separately in a given order with the previous part of the network frozen. An overview of the WM network is shown in Fig. 7.

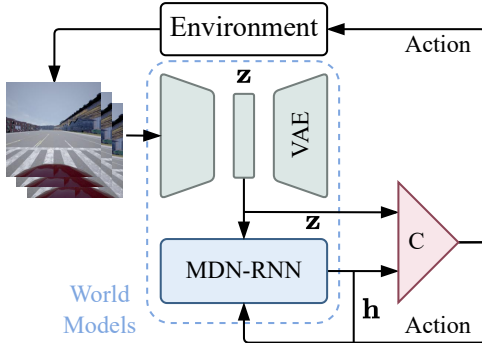


Fig. 7. Flow diagram of the World Models architecture.

In WM, the purpose of the mixture density network is to propagate the Gaussian Mixture that represents the learned latent state of the autoencoder and predict the hidden state. The MDN-RNN learns the transition $P(\mathbf{h}_t | \mathbf{a}_{t-1}, \mathbf{z}_{t-1}, \mathbf{h}_{t-1})$ that predicts the next hidden state \mathbf{h}_{t+1} that is concatenated with the previous latent encoding \mathbf{z}_t for controller input. The output action produced is defined as $\mathbf{a}_t = W_c[\mathbf{z}_{t-1}, \mathbf{h}_t] + \mathbf{b}_c$.

We adapt the WM architecture for the new scenario. First, the autoencoder part is modified to accommodate different image sizes, and more convolutional layers (apart from the reparametrization part) since the original input for the WM included 64×64 game screenplay, while we used 256×256 camera images. Both WM and CARNet autoencoders share identical convolutional encoder/decoder structure for fair comparison. Second, since this paper is focused on exploring latent

representations, the action-conditioning is removed from the recurrent predictions for the case of imitation learning, so that the recurrent part models the transition $T(\mathbf{z}_{t+1} | \mathbf{z}_t, \mathbf{h}_{t+1})$. Introducing action conditioning would bias the model toward learning the action dynamics, and it would be hard to show the improvements in the quality of the learned latent dynamics (see Section III-B). The controller parts of both networks are mostly identical layer-wise, with the only difference being the size of the input layers since WM uses hidden vectors of larger size — the hidden size of MDN-RNN that propagates the Gaussian mixture is 256, so the size of the input tensor to the controller network is $128 + 256 = 384$.

C. Reinforcement Learning

We have carried out the data collection and reinforcement learning training in the CARLA environment [33]. We modified the OpenAI Gym wrapper [39] for the CARLA simulator and used the customized version as an interface for the environment required for generating data for our learning algorithms. The reward function used for training is given as

$$r = 200 r_{\text{collision}} + v_{\text{lon}} + 10 \frac{S}{S_{\text{des}}} r_{\text{fast}} + 40 r_{\text{out}} - 5\alpha^2 + 0.2 r_{\text{lat}} - 0.1, \quad (10)$$

where $r_{\text{collision}}$ is set to -1 if the vehicle collides; else, it is set to 0 ; v_{lon} is the magnitude of the projection of the vehicle velocity vector along the direction connecting the vehicle and the nearest next way-point; r_{fast} is -1 when the car is faster than the desired speed else it is 0 ; r_{out} is -1 when the vehicle is out of the lane; α is the steering angle; r_{lat} refers to the lateral acceleration $= \alpha v^2$; the constant -0.1 is to make sure that the vehicle does not remain standstill. The penalty r_{fast} is either 0 or -1 , which acts as a constraint for over-speeding. Note that the coefficient for r_{out} is relatively large, as going out-of-lane causes a termination of the episode. Thus, the negative reward is only experienced once during an episode. Furthermore, a weight factor derived from normalizing the vehicle's speed S by the desired speed S_{des} (30 Km/h) is added to r_{fast} ; otherwise, the reward function would encourage a full-throttle policy. The action space is the same as in the imitation learning case (see Section IV-A) i.e., nine discrete actions corresponding to different combinations of steering ($[-0.2, 0.0, 0.2]$ rad) and acceleration ($[-3, 0.0, 3]$ m/s). Since the action space is discrete, we have used the DQN [40] algorithm for training the RL model. The hyper-parameters for the DQN model are shown in Table V.

D. Real World Data Evaluation

For the real-world evaluation, we have used the Udacity dataset [41]. In order to match the simulated dataset scenario and structure, the extracted images were resized to 256×256 dimensions and converted to grayscale. Since the Udacity dataset does not have a global shutter, resulting in camera and sensor timestamp mismatch, front camera timestamps were chosen as the reference ones, and closest images and sensor data were selected in relation to that timestamp. We post-processed throttle, steering, and brake values that were

¹<https://github.com/apak-00/cdae>

extracted from the rosbag file. The post-processing step is as follows: brake and throttle were discretized to match the CARLA scenario, in the range $[0, 1]$, and the steering wheel angle was normalized by dividing it by the steering wheel ratio of the car used in dataset collection, resulting in a normalized range of $[-1, 1]$.

V. RESULTS

This section presents the results from two different experiments, corresponding to imitation and reinforcement learning. In the first case, we explore autonomous driving in an imitation learning setting, which involves predicting the vehicle's actions (acceleration, braking, and throttle) from a sequence of four images from a front-facing camera. In the second scenario, we explore realistic autonomous driving scenarios in the CARLA environment [33] within the reinforcement learning setting. In both scenarios, the learned latent vectors are used to predict the vehicle's actions. Finally, we compare the performance of CARNet and WM in real-world data using Udacity dataset [41].

A. Ablation Analysis

We performed ablation studies to select the best network configuration and hyper-parameters. Ablation studies were performed on the simulated dataset. The parameters of the ablation study are summarized in Table III and selected parameters are highlighted in bold.

TABLE III
ABLATION STUDIES OVERVIEW

Parameters	Latent Size	RNN Unit	Loss Function
Range	[64, 128, 256]	[LSTM, GRU]	[MSE, MS-SSIM]

First, during the initial experiments LSTM was replaced in favor of GRU, as the former showed heavy over-fitting behavior (see Fig. 9). Second, we selected MS-SSIM for the image reconstruction loss as MSE often resulted in mode collapse and blurry image reconstruction since it did not impose any structural constraints on the decoded image. Lastly, we tested various latent sizes for the autoencoder and hidden vector sizes for RNN. While reducing the latent size did address the over-fitting problem, reducing the size further led to low representation capacity (summarized in Fig. 8). Hence, we chose a latent size of 128. Moreover, in imitation learning experiments, the performance difference between 128 and 256 latent sizes appeared to be negligible (see Section IV-A). Thus, a latent size of 128 provides a good trade-off between the representation capacity and the number of trainable parameters.

B. Separate and Ensemble Training (Autoencoder & Recurrent Parts)

Recall that the CARNet model consists of an autoencoder with a Recurrent Neural Network (RNN) trained together. In order to speed up the training process, we pre-trained the autoencoder and fine-tuned the weights as part of the whole

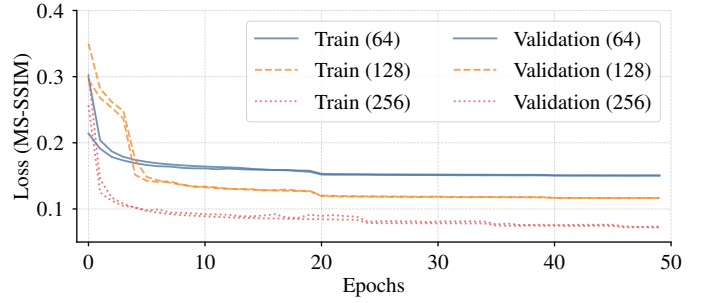


Fig. 8. MS-SSIM loss for autoencoder reconstructions of various latent variable sizes. Note that the range for the MS-SSIM loss is $[0, 1]$, where 0 corresponds to perfect structure match, while 1 shows complete mismatch, accordingly. A nearly linear relation can be observed between the latent variable size and final reconstruction quality.

TABLE IV
LEARNING HYPERPARAMETERS

Hyperparameter	Value
Input image size	256x256
Autoencoder latent size	128
GRU hidden size	128
RNN time-steps	4
Optimizer	Adam
Learning rate (scheduled)	10^{-3}
Batch size	64

TABLE V
DQN HYPERPARAMETERS

Hyperparameter	Value
Training steps	500000
Buffer size	5000
Optimizer	Adam
Learning rate	5×10^{-3}
Batch size	64
N-step Q	1
Prioritized replay	True
Replay α	0.6
Replay β	0.4

network i.e., AE + RNN (see Fig. 3). First, we present the results of the pre-training procedure. Note that we also used the convolution attention mechanism (see Fig. 4) with the autoencoder model as explained in Section III-A. Fig. 10 (latent size 128) shows the training and validation curve for pretrained models, which suggests that there is no over-fitting at the pre-training stage. Example reconstructions for both simulated and real data after pre-training stage are shown in Fig. 11.

As can be seen in Fig. 11, the autoencoder is capable of adequately capturing all necessary parts of the source image. Nonetheless, it is important to note that our main aim was to learn latent dynamics rather than ideal image reconstruction. After pre-training the autoencoder, we combined it with the RNN and trained them together without freezing the weights of the autoencoder. This is unlike the WM, where each part of the network is trained in isolation in a sequential manner, i.e., first the autoencoder, then the recurrent part with autoencoder weights frozen. The training losses for the CARNet with GRU are shown in Fig. 13. The GRU performed better than LSTM both in terms of final loss value and overfit. The slight overfit in the image reconstruction appears due to the dataset size. Qualitatively, Fig. 12 shows image reconstructions from predicted latent space. The quantitative differences in the learned latent variables become more apparent when the imitation learning network is added on top, as shown in the next subsection.

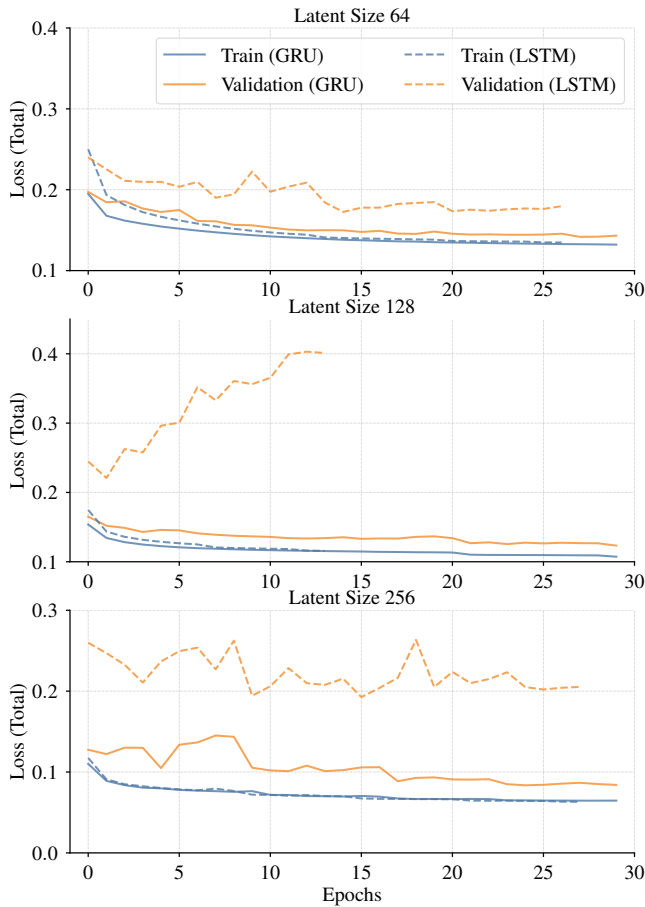


Fig. 9. LSTM vs. GRU varying latent variable size training and validation curves. Note that LSTM training often triggered early stopping criteria (no decrease in validation loss, even with learning rate scheduling and showed high tendency to overfitting compared to GRU. Both RNN architectures were trained under the same set of hyperparameters.

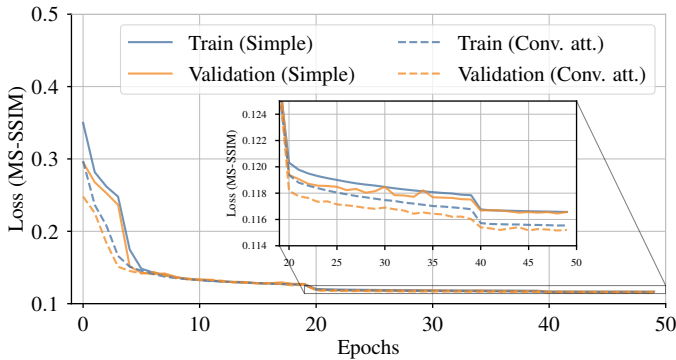


Fig. 10. Two autoencoder architectures training results. Adding convolutional self-attention after the image input does not result in any significant qualitative or quantitative improvement in image reconstruction.

C. Imitation Learning (CARLA)

The imitation classification results of the proposed architecture CARNet (Fig. 3) and the baseline model (WM) is shown in Table VI. The CARNet had a classification validation accuracy of $\approx 77\%$, while WM performance was $\approx 71\%$. The proposed CARNet model performed significantly better than the World Models (WM) while having ≈ 2.5 times fewer

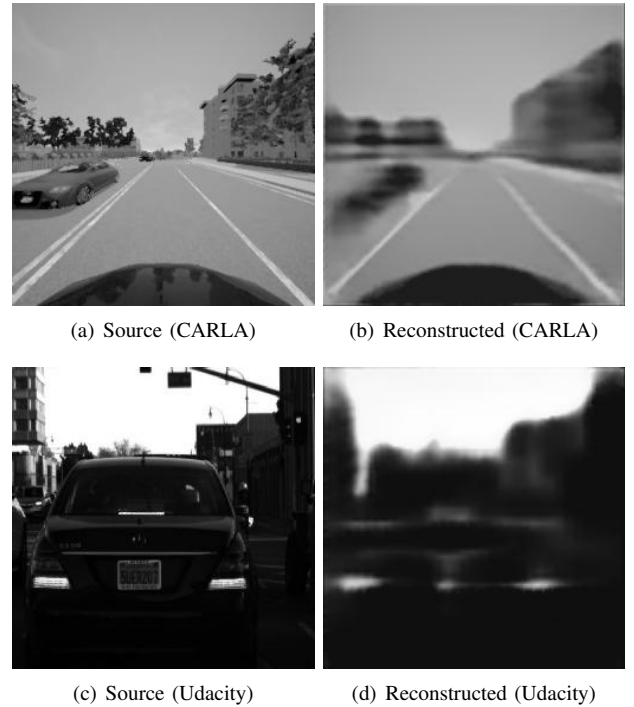


Fig. 11. Autoencoder reconstruction examples. We omit reconstructions for convolution attention-based autoencoder since the difference is imperceptible to human eye.

parameters. Moreover, neither increasing the latent size to 256 (Fig. 14) nor adding convolutional self-attention resulted in a noticeable improvement in classification accuracy (Table VI).

TABLE VI
IMITATION LEARNING RESULTS COMPARISON (CARLA SIMULATED DATASET).

Model	Classification Accuracy%
World Models	71.37 ± 0.52
CARNet (latent size = 128)	77.08 ± 0.51
CARNet (latent size = 256)	77.30 ± 0.41
CARNet (latent size = 128) + Conv. self-attention	76.61 ± 0.39

D. Imitation Learning (Udacity Dataset)

TABLE VII
IMITATION LEARNING RESULTS COMPARISON (UDACITY DATASET).

Model	Classification Accuracy%
World Models	45.92 ± 1.66
CARNet (latent size = 128)	54.24 ± 1.24
CARNet (latent size = 128), simulation to real*	57.02 ± 1.53
CARNet (latent size = 256)	59.80 ± 1.10

* Network was pre-trained on a simulated and fine-tuned on the real-world dataset.

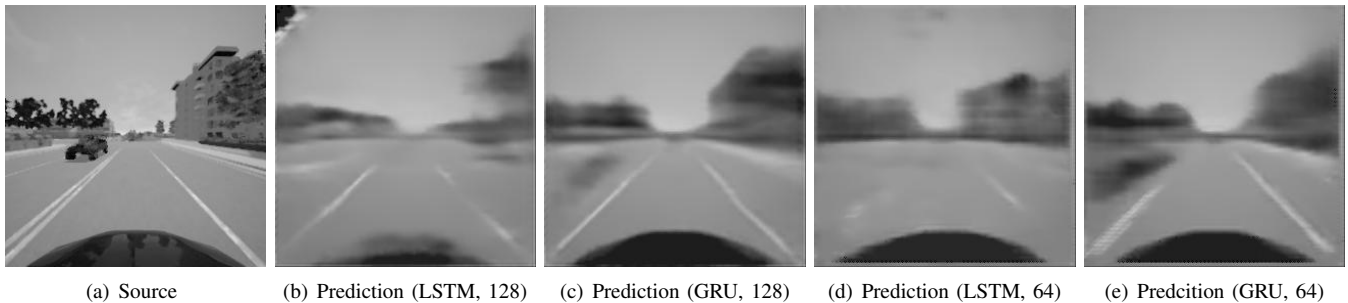


Fig. 12. Comparison of autoencoder reconstruction quality of 512, 128 and 64 latent size vectors. The corresponding training curves are shown in Fig. 13.

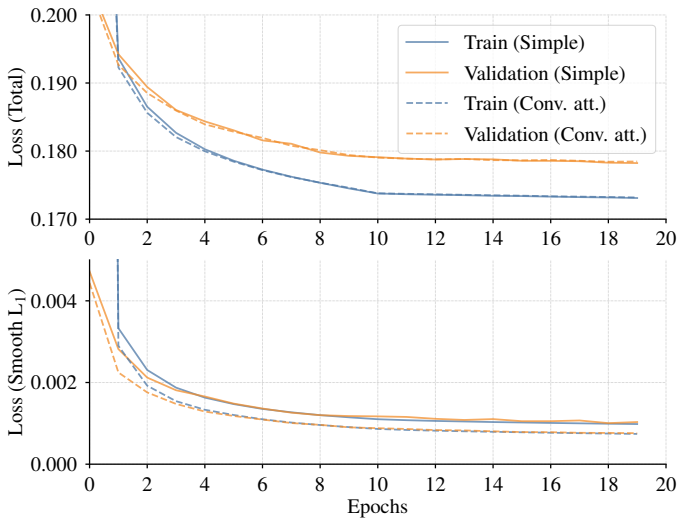


Fig. 13. GRU architecture training results. Similar to autoencoder part, adding convolutional self-attention did not yield performance improvements.

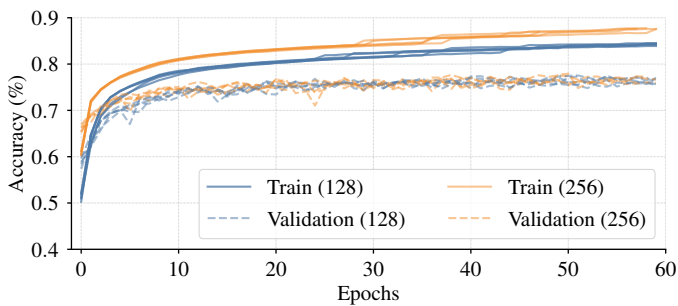


Fig. 14. Imitation learning autopilot action classification accuracy. Results are ran five times with resulting accuracies presented Table VI.

The proposed CARNet showed an even better performance margin on real-world data (Udacity dataset). While the overall performance accuracies were less than the ones for the simulated dataset, the CARNet outperformed WM by about 8% for a latent size of 128. Moreover, in sim-to-real training, when the network was pre-trained on a CARLA dataset and then fine-tuned on the Udacity dataset, the network consistently showed noticeably better performance compared to when trained entirely on real-world data. A performance drop on the real dataset is expected since real data is more diverse, e.g., texture, shadows, camera over/under-exposure, etc. Ad-

ditionally, since the minimum possible configuration of the network was explored, the autoencoder might lack the capacity to reconstruct real images compared to simulation quality data. While for simulated data there were no performance gains observed when going from a 128 to a 256 latent variable size, for real-world data increasing the latent variable size resulted in about 5% performance gain as shown in Table VII.

E. Reinforcement Learning

For the reinforcement learning task, we followed the same architecture shown in Fig. 6. The backbone networks (CARNet

TABLE VIII
REINFORCEMENT LEARNING RESULTS COMPARISON.

Model	World Models	CARNet
Reward	2508.77 \pm 249.2	3057.88 \pm 155.56

or WM) were frozen, and only the fully connected layers were trained. However, the fully connected layers were trained using the temporal difference error from the DQN algorithm. As shown in Table VIII, the proposed CARNet model performed better than WM. The main difference between the proposed CARNet model and the WM is that the CARNet is conditioned on the history of sensor values (i.e. $P(\mathbf{z}_{t+1}|\mathbf{s}_t, \mathbf{z}_t, \mathbf{h}_t)$) rather than the history of actions (i.e. $P(\mathbf{z}_{t+1}|\mathbf{a}_t, \mathbf{z}_t, \mathbf{h}_t)$, see Section III-B). Conditioning on the sensor data has two advantages: First, by omitting sensor-action transformations, we avoid the influence of action discretization on the state transition function. In other words, if we use the action data, then pre-processing steps such as discretization (from continuous actions) should be applied. Depending on the granularity of the action discretization, the quality of the state transition estimation can deteriorate. Second, using raw continuous sensor measurements is a more natural way of handling data for autonomous driving, which also avoids additional task-specific post-processing.

VI. CONCLUSION

This paper presents a novel approach for learning latent dynamics in an autonomous driving scenario. The proposed architecture follows a dynamic convolutional autoencoder structure where the neural network consists of convolutional and recurrent architectures that are trained together. The combined

architecture provides several advantages, such as reduced trainable parameters and additional continuity constraints on the latent space representation. We showed the efficacy of the proposed model with respect to the established World Models (WM) architecture in both imitation and reinforcement learning scenarios. Evaluation was performed using both simulated data and real-world driving data. While simpler, the proposed model outperforms the state-of-the-art (WM) in both imitation learning and reinforcement learning scenarios. In imitation learning (cast as a classification problem), the proposed model performance is $\approx 6\%$ and $\approx 8\%$ better than WM for simulated real data, respectively. In terms of reinforcement learning, the average reward learned through the proposed model is ≈ 549 (or 22%) higher than WM. For future work, we aim to explore the generalization and robustness of the proposed model in different scenarios, for example, different town or weather and lighting conditions.

ACKNOWLEDGMENT

The authors would like to thank Vlachas Pantelis Rafail for providing valuable advice on recurrent network training and Brian Lee for evaluating the World Models performance on the simulated dataset. We also like to thank Mahdi Ghanei for helping with the synthetic data generation using the CARLA environment.

REFERENCES

- [1] T. Lesort, N. Díaz-Rodríguez, J.-F. Goudou, and D. Filliat, "State Representation Learning for Control: An Overview," *Neural Networks*, vol. 108, p. 379–392, Dec 2018. [Online]. Available: <http://dx.doi.org/10.1016/j.neunet.2018.07.006>
- [2] P. J. Werbos, "Learning How the World Works: Specifications for Predictive Networks in Robots and Brains," in *Proceedings of IEEE International Conference on Systems, Man and Cybernetics*, NY, 1987.
- [3] D. Silver, H. Hasselt, M. Hessel, T. Schaul, A. Guez, T. Harley, G. Dulac-Arnold, D. Reichert, N. Rabinowitz, A. Barreto *et al.*, "The Predictron: End-to-end Learning and Planning," in *Proceedings of the 34th International Conference on Machine Learning*, ser. Proceedings of Machine Learning Research, D. Precup and Y. W. Teh, Eds., vol. 70. PMLR, 06–11 Aug 2017, pp. 3191–3199. [Online]. Available: <https://proceedings.mlr.press/v70/silver17a.html>
- [4] R. Shadmehr and S. Mussa-Ivaldi, *Biological Learning and Control: How the Brain Builds Representations, Predicts Events, and Makes Decisions*. MIT Press, 2012.
- [5] L. Girin, S. Leglaive, X. Bie, J. Diard, T. Hueber, and X. Alameda-Pineda, "Dynamical Variational Autoencoders: A Comprehensive Review," *Foundations and Trends® in Machine Learning*, vol. 15, no. 1–2, p. 1–175, 2021. [Online]. Available: <http://dx.doi.org/10.1561/22000000089>
- [6] D. Ha and J. Schmidhuber, "Recurrent World Models Facilitate Policy Evolution," in *Advances in Neural Information Processing Systems*, S. Bengio, H. Wallach, H. Larochelle, K. Grauman, N. Cesa-Bianchi, and R. Garnett, Eds., vol. 31, 2018.
- [7] T. Salimans, "A Structured Variational Auto-encoder for Learning Deep Hierarchies of Sparse Features," *arXiv preprint arXiv:1602.08734*, 2016.
- [8] J. Chung, K. Kastner, L. Dinh, K. Goel, A. C. Courville, and Y. Bengio, "A Recurrent Latent Variable Model for Sequential Data," *Advances in Neural Information Processing Systems*, vol. 28, pp. 2980–2988, 2015.
- [9] D. P. Kingma and M. Welling, "An Introduction to Variational Autoencoders," *Foundations and Trends® in Machine Learning*, vol. 12, no. 4, p. 307–392, 2019. [Online]. Available: <http://dx.doi.org/10.1561/22000000056>
- [10] A. Vaswani, N. Shazeer, N. Parmar, J. Uszkoreit, L. Jones, A. N. Gomez, Ł. Kaiser, and I. Polosukhin, "Attention Is All You Need," *Advances in Neural Information Processing Systems*, vol. 30, 2017.
- [11] Y. Tang, D. Nguyen, and D. Ha, "Neuroevolution of Self-Interpretable Agents," in *Proceedings of the 2020 Genetic and Evolutionary Computation Conference*, 2020, pp. 414–424.
- [12] C. Gelada, S. Kumar, J. Buckman, O. Nachum, and M. G. Bellemare, "DeepMDP: Learning Continuous Latent Space Models for Representation Learning," in *International Conference on Machine Learning*, PMLR, 2019, pp. 2170–2179.
- [13] C. Chen, A. Seff, A. Kornhauser, and J. Xiao, "Deepdriving: Learning Affordance for Direct Perception in Autonomous Driving," in *Proceedings of the IEEE International Conference on Computer Vision*, 2015, pp. 2722–2730.
- [14] C. Ahlstrom, T. Victor, C. Wege, and E. Steinmetz, "Processing of Eye/Head-Tracking Data in Large-Scale Naturalistic Driving Data Sets," *IEEE Transactions on Intelligent Transportation Systems*, vol. 13, no. 2, pp. 553–564, 2011.
- [15] A. Swief, A. El-Zawawi, and M. El-Habrouk, "A Survey of Model Predictive Control Development in Automotive Industries," in *2019 International Conference on Applied Automation and Industrial Diagnostics (ICAAID)*, vol. 1, 2019, pp. 1–7.
- [16] N. Wahlström, T. B. Schön, and M. P. Deisenroth, "From Pixels to Torques: Policy Learning with Deep Dynamical Models," in *Deep Learning Workshop at ICML 2015*, 2015. [Online]. Available: <https://arxiv.org/abs/1502.02251>
- [17] M. Watter, J. Springenberg, J. Boedecker, and M. Riedmiller, "Embed to Control: A Locally Linear Latent Dynamics Model for Control from Raw Images," *Advances in Neural Information Processing Systems*, vol. 28, 2015.
- [18] V. Pătrăucean, A. Handa, and R. Cipolla, "Spatio-Temporal Video Autoencoder with Differentiable Memory," in *International Conference on Learning Representations (ICLR) Workshop*, 2016.
- [19] W. Sun, A. Venkatraman, B. Boots, and J. A. Bagnell, "Learning to Filter with Predictive State Inference Machines," in *International Conference on Machine Learning*. PMLR, 2016, pp. 1197–1205.
- [20] S. Chiappa, S. Racanière, D. Wierstra, and S. Mohamed, "Recurrent Environment Simulators," in *5th International Conference on Learning Representations, ICLR 2017, Toulon, France, April 24-26, 2017, Conference Track Proceedings*, 2017. [Online]. Available: <https://arxiv.org/abs/1704.02254>
- [21] A. Graves, "Generating Sequences With Recurrent Neural Networks," *arXiv e-prints*, p. arXiv:1308.0850, Aug. 2013.
- [22] M. Kempka, M. Wydmuch, G. Runc, J. Toczek, and W. Jaśkowski, "Vizdoom: A Doom-Based AI Research Platform For Visual Reinforcement Learning," in *2016 IEEE Conference on Computational Intelligence and Games (CIG)*, 2016, pp. 1–8.
- [23] D. Hafner, T. Lillicrap, I. Fischer, R. Villegas, D. Ha, H. Lee, and J. Davidson, "Learning Latent Dynamics for Planning from Pixels," in *Proceedings of the 36th International Conference on Machine Learning*, ser. Proceedings of Machine Learning Research, K. Chaudhuri and R. Salakhutdinov, Eds., vol. 97. PMLR, 09–15 Jun 2019, pp. 2555–2565. [Online]. Available: <https://proceedings.mlr.press/v97/hafner19a.html>
- [24] S. W. Kim, Y. Zhou, J. Phillion, A. Torralba, and S. Fidler, "Learning to Simulate Dynamic Environments with GameGAN," in *IEEE Conference on Computer Vision and Pattern Recognition (CVPR)*, Jun. 2020.
- [25] S. Hochreiter and J. Schmidhuber, "Long Short-Term Memory," *Neural Computation*, vol. 9, no. 8, pp. 1735–1780, 1997.
- [26] S. W. Kim, J. Phillion, A. Torralba, and S. Fidler, "DriveGAN: Towards a Controllable High-Quality Neural Simulation," in *IEEE Conference on Computer Vision and Pattern Recognition (CVPR)*, Jun. 2021.
- [27] I. Higgins, L. Matthey, A. Pal, C. Burgess, X. Glorot, M. M. Botvinick, S. Mohamed, and A. Lerchner, "Beta-VAE: Learning Basic Visual Concepts with a Constrained Variational Framework," in *5th International Conference on Learning Representations, ICLR 2017, Toulon, France, April 24-26, 2017, Conference Track Proceedings*. OpenReview.net, 2017. [Online]. Available: <https://openreview.net/forum?id=Sy2fzU9gl>
- [28] T. Karras, S. Laine, and T. Aila, "A Style-Based Generator Architecture for Generative Adversarial Networks," in *Proceedings of the IEEE/CVF Conference on Computer Vision and Pattern Recognition*, 2019, pp. 4401–4410.
- [29] T. Karras, S. Laine, M. Aittala, J. Hellsten, J. Lehtinen, and T. Aila, "Analyzing and Improving the Image Quality of StyleGAN," in *Proceedings of the IEEE/CVF Conference on Computer Vision and Pattern Recognition*, 2020, pp. 8110–8119.
- [30] A. B. L. Larsen, S. K. Sønderby, H. Larochelle, and O. Winther, "Autoencoding beyond Pixels Using a Learned Similarity Metric," in *Proceedings of the 33rd International Conference on International Conference on Machine Learning - Volume 48*, ser. ICML'16, 2016, p. 1558–1566.

- [31] Z. Wang, E. P. Simoncelli, and A. C. Bovik, "Multiscale Structural Similarity for Image Quality Assessment," in *The Thirty-Seventh Asilomar Conference on Signals, Systems & Computers, 2003*, vol. 2, 2003, pp. 1398–1402.
- [32] N. Parmar, P. Ramachandran, A. Vaswani, I. Bello, A. Levskaya, and J. Shlens, "Stand-Alone Self-Attention in Vision Models," in *Advances in Neural Information Processing Systems 32: Annual Conference on Neural Information Processing Systems 2019, NeurIPS 2019, December 8-14, 2019, Vancouver, BC, Canada*, H. M. Wallach, H. Larochelle, A. Beygelzimer, F. d'Alché-Buc, E. B. Fox, and R. Garnett, Eds., 2019, pp. 68–80. [Online]. Available: <https://proceedings.neurips.cc/paper/2019/hash/3416a75f4cea9109507cacd8e2f2aefc-Abstract.html>
- [33] A. Dosovitskiy, G. Ros, F. Codevilla, A. Lopez, and V. Koltun, "CARLA: An Open Urban Driving Simulator," in *Conference on Robot Learning*. PMLR, 2017, pp. 1–16.
- [34] S. Griffith, K. Subramanian, J. Scholz, C. L. Isbell, and A. L. Thomaz, "Policy Shaping: Integrating Human Feedback with Reinforcement Learning," in *Advances in Neural Information Processing Systems*, 2013, pp. 2625–2633.
- [35] P. F. Christiano, J. Leike, T. Brown, M. Martic, S. Legg, and D. Amodei, "Deep Reinforcement Learning from Human Preferences," in *Advances in Neural Information Processing Systems*, 2017, pp. 4299–4307.
- [36] D. Silver, A. Huang, C. J. Maddison, A. Guez, L. Sifre, G. Van Den Driessche, J. Schrittwieser, I. Antonoglou, V. Panneershelvam, M. Lanctot *et al.*, "Mastering the Game of Go with Deep Neural Networks and Tree Search," *Nature*, vol. 529, no. 7587, p. 484, 2016.
- [37] O. Vinyals, I. Babuschkin, W. M. Czarnecki, M. Mathieu, A. Dudzik, J. Chung, D. H. Choi, R. Powell, T. Ewalds, P. Georgiev *et al.*, "Grandmaster Level in StarCraft II Using Multi-Agent Reinforcement Learning," *Nature*, vol. 575, no. 7782, pp. 350–354, 2019.
- [38] S. Nagesh Rao, H. E. Tseng, and D. Filev, "Autonomous highway driving using deep reinforcement learning," in *2019 IEEE International Conference on Systems, Man and Cybernetics (SMC)*. IEEE, 2019, pp. 2326–2331.
- [39] J. Chen, S. E. Li, and M. Tomizuka, "Interpretable End-to-End Urban Autonomous Driving with Latent Deep Reinforcement Learning," *IEEE Transactions on Intelligent Transportation Systems*, 2021.
- [40] V. Mnih, K. Kavukcuoglu, D. Silver, A. Graves, I. Antonoglou, D. Wierstra, and M. Riedmiller, "Playing Atari with Deep Reinforcement Learning," *arXiv preprint arXiv:1312.5602*, 2013.
- [41] Y. Hou, Z. Ma, C. Liu, and C. C. Loy, "Learning to Steer by Mimicking Features from Heterogeneous Auxiliary Networks," in *Proceedings of the Thirty-Third AAAI Conference on Artificial Intelligence and Thirty-First Innovative Applications of Artificial Intelligence Conference and Ninth AAAI Symposium on Educational Advances in Artificial Intelligence*, ser. AAAI'19/IAAI'19/EAAI'19. AAAI Press, 2019. [Online]. Available: <https://doi.org/10.1609/aaai.v33i01.33018433>